Spectroscopic line parameters of water vapor for rotation-vibration transitions near 7180 cm^{-1}

D. Lisak

Instytut Fizyki, Uniwersytet Mikołaja Kopernika, ul. Grudziadzka 5/7, 87-100 Toruń, Poland

D. K. Havey and J. T. Hodges

Process Measurements Division, National Institute of Standards and Technology, 100 Bureau Drive, Gaithersburg, Maryland 20899, USA

We present low uncertainty measurements of line parameters for 15 rotation-vibration transitions of water vapor in the wave number range of 7170.27–7183.02 cm^{-1}. These experiments incorporated frequency-stabilized cavity ring-down spectroscopy and a primary standard humidity generator which produced a stable and accurately known amount of water vapor in a nitrogen carrier gas stream. Intensities and line shape factors were derived by fitting high-resolution spectra to spectral models that account for collisional narrowing and speed-dependent broadening and shifting effects. For most transitions reported here, we estimate the relative combined standard uncertainty of the line intensities to be <0.4%, of which approximately one half this value we ascribe to limited knowledge of the line shape. Our measured intensities and broadening parameters are compared to experimental and theoretical literature values. Agreement between our experimental intensity measurements and those derived by recent *ab initio* calculations of the dipole moment surface of water vapor is within 1.5%.

PACS number(s): 33.20.Vq, 33.70.Jg

I. INTRODUCTION

A quantitative understanding of the rotation-vibration spectrum of water is critical to many scientific and technical fields. Water vapor dominates the absorption of incoming (solar) and outgoing (thermal) radiations in the Earth's atmosphere, and its rotation-vibration spectrum is relevant to remote sensing techniques in which the atmospheric compositions of water vapor and other species are retrieved from measured absorption spectra [1]. Further, there are many applications where the measurement of water vapor amount via absorption spectroscopy provides essential information for system quantification, control, and optimization. Examples include propulsion [2], combustion [3–6], ultrahigh purity gases for semiconductor manufacturing [7,8], particle synthesis [9], and human breath analysis [10]. Increasing demands on sensitivity and accuracy in these diverse fields motivate complementary experimental and theoretical studies leading to a comprehensive and quantitative description of the rotation-vibration spectrum of water vapor. To be most useful, this description must be valid over a wide range of wavelength, temperature, pressure, and gas mixture composition.

A thorough understanding of the water vapor rotation-vibration spectrum includes knowledge (expected values and uncertainties) of the positions, intensities, and line shape coefficients of all relevant transitions. Significant progress has recently been made on *ab initio* line lists derived from variational calculations that incorporate accurate potential energy surfaces [11]. These line lists enable prediction of transition wave numbers at the 0.02 cm^{-1} level, comparable to experimental uncertainties for weak and blended lines. Similarly, recent advances in the calculation of dipole moment surfaces such as the Barber-Tennyson 2 (BT2) model [12] and the core correlation valence-only relativistic (CVR) model [13] are expected to improve theoretical predictions of water vapor line intensities.

Line lists based on *ab initio* calculations require benchmark intensity data against which they can be validated. However because of difficulties in delivering a water vapor sample of known concentration to an absorption spectrometer, the measurement of absorption coefficients for water vapor is problematic and often fraught with systematic uncertainty. In the case of optically thick transitions, relatively small concentrations of water vapor must be sampled. This requirement precludes accurate pressure measurement and renders measurements sensitive to relatively slow and difficult-to-control adsorption and desorption processes that involve the water vapor and internal surfaces of the sample volume. Many laboratory techniques are also sensitive to the presence of ambient water vapor and temperature gradients within the sample volume, thus increasing the combined uncertainty in water vapor concentration (and hence line intensity).

The validation and application of nonstandard line shape models such as those accounting for collisional narrowing and speed-dependent broadening and shifting effects are critical to the realization of water vapor intensity measurements at the subpercent relative uncertainty level [14,15]. We have recently measured rotation-vibration intensities [16] and pressure broadening parameters [17] for water vapor in the 930 nm region by integrating high-resolution cavity ring-down spectroscopy measurements, detailed line shape analyses, and sample generation methods directly traceable to primary standards of humidity. In the first study we measured line intensities with relative standard uncertainties approaching 0.5% [16], and subsequently Shirin *et al.* [11] presented *ab initio* dipole moment surface calculations of intensities that were within 3% of our measured values. In the second study the relative standard deviation between our line broadening measurements and theoretical calculations was 1.7% with a mean relative difference of ~0.6% [17].

In this paper we present line intensity and nitrogen-broadened line shape parameter measurements for a number
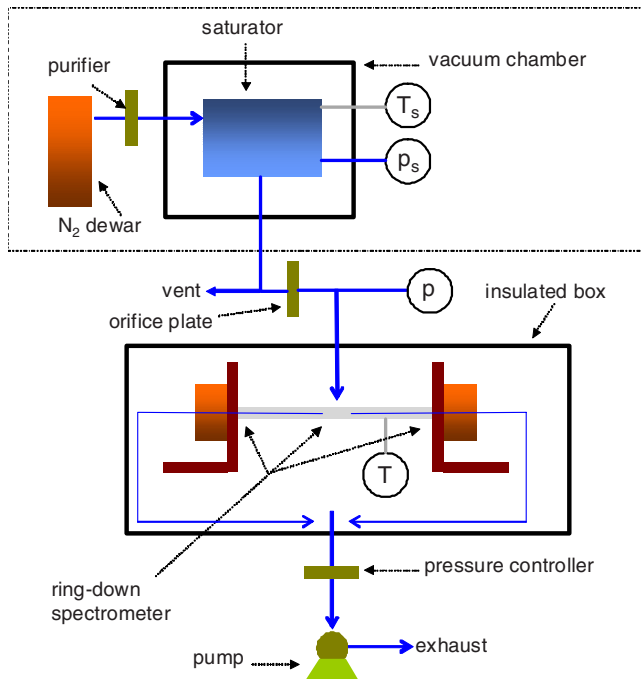
FIG. 1. (Color online) Schematic diagram illustrating the interface of the primary standard humidity generator (LFPG) to the ring-down spectrometer. The LFPG comprises the components within the dashed bounding box. The gas flow path is indicated by the arrowed lines.

of near-infrared rotation-vibration transitions of water vapor. High-resolution absorption spectra of water vapor/N_2 mixtures were acquired using the frequency-stabilized cavity ring-down spectroscopy (FS-CRDS) technique [18,19]. Below we discuss the measurement technique and line shape analysis, and we compare our results to literature data and theoretical calculations.

II. EXPERIMENTAL APPARATUS

The experimental apparatus, which is located at the National Institute of Standards and Technology (NIST) in Gaithersburg, Maryland, USA, comprises a primary standard humidity generator known as the low frost-point generator (LFPG) [20,21] and a FS-CRDS apparatus [22]. The former provides a known quantity of water vapor in a steady flow of nitrogen carrier gas and the latter is the spectrometer used to measure the absorption spectrum of water vapor. The principal components of the humidity generation system and gas sampling scheme are shown in Fig. 1. The FS-CRDS apparatus for probing water vapor includes a single-mode continuous-wave distributed feedback diode laser which selectively pumps individual longitudinal modes of a length-stabilized ring-down cavity. The present spectrometer is identical to that previously described, with the exception of a modified gas flow configuration, and the incorporation of an insulating enclosure designed to minimize diurnal fluctuations in the system temperature. As shown in Fig. 1, the sample gas was introduced into the middle of the ring-down cell and symmetrically exhausted out the two ends of the

cavity. This new arrangement reduced the background water vapor contribution emanating from the cell walls and ensured that gas flow swept all internal surfaces bounded by the ring-down cavity mirrors, eliminating so-called "dead volumes" of stagnant gas where the local water vapor concentration is driven by diffusion to or from the bounding metal surfaces. Gas flow was drawn through the ring-down cell by a diaphragm vacuum pump, giving a volumetric flow rate of 0.85 l min^{-1} (at standard temperature and pressure conditions) for all line parameter measurements reported here. A critical-flow orifice plate between the LFPG (see Fig. 1) and ring-down cavity maintained a large pressure drop between the two systems, and a servo-controlled solenoid-actuated valve regulated the gas pressure in the ring-down cell. We measured the sample gas pressure, p, with a capacitance diaphragm gauge [$u_r(p) < 0.07\%$], and temperature, T, was measured with a 2.4 kΩ thermistor mounted in good thermal contact with the outer surface of the stainless steel tube comprising the sample cell. The thermistor temperature uncertainty was $u(T) = 15$ mK, and two thermocouples were mounted at opposite ends of the ring-down spectrometer and indicated a maximum temperature difference of 30 mK.

A. Primary standard humidity generator

The LFPG is a primary standard humidity generator developed and maintained at NIST to support hygrometric measurements in ultradry gas streams. This system produces steady flow mixtures of trace water vapor in nitrogen over the water vapor molar fraction range, x_w $=4$ nmol mol^{-1}–4 mmol mol^{-1}. The humidity level delivered by the LFPG can be modeled in terms of relatively simple thermodynamic relations, and its output has been validated against NIST's primary gravimetric humidity standards [23]. The LFPG consists of an isothermal copper saturator with actively controlled temperature (with a precision of 2 mK) over the range of −101 to −5 °C. The saturator has a 4-m-long channel filled with ice over which nitrogen carrier gas flows. The long flow path and isothermal conditions (maximum temperature difference of 10 mK) ensure that the water vapor content in the exiting gas stream is independent of gas flow rate. Thus the water vapor in the sample stream can be assumed to be in thermodynamic equilibrium with the ice-coated channel of the LFPG saturator, and the water vapor molar fraction in the output stream of the LFPG is given by $x_w = e_w(T_s)f(T_s, p_s)/p_s$, where e_w is the vapor pressure of hexagonal ice [24], T_s and p_s are the saturator temperature and pressure, respectively, and f is the enhancement factor accounting for nonideal gas and nonideal mixing effects [25]. In this study $f(T_s, p_s)$ is assumed to be that of air and is ~1.007. Over the range of measurements reported here, the relative combined standard uncertainty, $u_r(x_w)$, increases with decreasing x_w and varies from 0.21% at $x_w=3.3\times10^{-6}$ to 0.065% at $x_w=1.7\times10^{-3}$ [26]. In our previous study of water vapor line intensities [21] we used a portable humidity generator and a transfer-standard chilled-mirror hygrometer having $u_r(x_w)=0.4\%$. The present configuration eliminated this additional uncertainty since the FS-CRDS gas sampling system was connected directly to the output of the NIST primary standard humidity generator.

TABLE I. List of investigated water transitions with transition wave numbers, intensities at $T_r = 296$ K, lower state energy levels, and quantum assignments. Data are taken from HITRAN [31].

$\widetilde{\nu}_0$ (cm^{-1})	$S(T_r)$ cm^{-1}/(molecule cm^{-2})	E'' (cm^{-1})	V'	V''	Q'	Q''
7170.27781	1.969×10^{-21}	206.3014	101	0 0 0	2 2 1	3 2 2
7172.69909	3.288×10^{-22}	300.3623	200	0 0 0	3 3 0	4 2 3
7173.96018	2.683×10^{-23}	1059.8354	021	0 0 0	8 5 3	7 5 2
7174.13738	5.809×10^{-22}	95.1759	200	0 0 0	2 0 2	2 1 1
7175.49242	2.905×10^{-23}	1360.2354	101	0 0 0	9 4 6	9 4 5
7175.98676	2.715×10^{-22}	206.3014	101	0 0 0	3 0 3	3 2 2
7178.44584	1.493×10^{-22}	602.7735	101	0 0 0	6 2 5	6 2 4
7179.18718	6.011×10^{-23}	326.6255	200	0 0 0	4 2 2	5 1 5
7179.75201	2.299×10^{-22}	1216.1945	101	0 0 0	7 6 2	7 6 1
7180.39972	5.608×10^{-22}	224.8384	200	0 0 0	3 2 1	4 1 4
7180.61301	3.038×10^{-23}	1477.2974	101	0 0 0	9 5 5	9 5 4
7181.15578	1.505×10^{-20}	136.7617	101	0 0 0	2 0 2	3 0 3
7182.20911	1.541×10^{-21}	42.3717	200	0 0 0	1 0 1	1 1 0
7182.94962	3.752×10^{-21}	142.2785	101	0 0 0	2 1 2	3 1 3
7183.01579	4.115×10^{-22}	134.9016	101	0 0 0	2 1 2	3 1 3

B. Determination of line intensity

We modeled the measured FS-CRDS spectra, denoted by $[c\tau(\widetilde{\nu})]^{-1}$, as the sum of absorption line shape profiles superimposed on a linear baseline $n_0[c\tau(\widetilde{\nu})]^{-1} = \alpha(\widetilde{\nu}) + \mathcal{L}_b(\widetilde{\nu})\ell^{-1}$. Here n_0 is the broadband (nonresonant) index of refraction of the medium [27], c is the speed of light, τ is the measured ring-down time constant, ℓ is the cavity length, and $\mathcal{L}_b(\widetilde{\nu})$ is the effective base cavity loss comprising all losses other than local line absorption by the gas sample. This baseline term typically exhibits a weak wave number dependence and includes transmittance, absorbance, scattering, and diffraction losses associated with the ring-down mirrors, Rayleigh scattering by the medium, as well as far-wing absorption and continuum absorption by water vapor. Measurements of the empty cavity losses and inspection of fit residuals showed that etaloning in the baseline (caused by coupled cavity effects and manifest as a sinusoidally varying loss [28]) was negligible. From dispersion relations for the refractive index of nitrogen [29], we calculate that $1.8 \times 10^{-5} < (n_0 - 1) < 7.2 \times 10^{-5}$ for all sample conditions considered here and therefore we set $n_0 = 1$ in the spectral analysis. The spectrum wave number $\widetilde{\nu}$ equals $\widetilde{\nu}_s + q\nu_{\text{FSR}}/c$, in which $\widetilde{\nu}_s$ is the laser's starting wave number measured by a wave meter, ν_{FSR} is the cavity free spectral range having dimensions of frequency q is the index counting the number of ring-down cavity longitudinal mode orders through which the laser is tuned relative to the beginning of the scan. We note that in the FS-CRDS technique, the comb of resonant frequencies of the ring-down cavity is actively stabilized using a frequency-stabilized reference laser, thus giving rise to a highly linear and precise spectrum axis having a wave number resolution $< 3 \times 10^{-5}$ cm^{-1} (~ 1 MHz) [30]. We used the ideal gas relation (which is a good assumption for mixtures of water vapor and nitrogen in the temperature and pressure range considered here) $x_w p(k_B T)^{-1}$ to calculate the water vapor

number density, n, in which k_B is the Boltzmann constant. The line area $\mathcal{A}$ is found by evaluating $\int d\widetilde{\nu}\alpha(\widetilde{\nu} - \widetilde{\nu}_0)$, where α is the absorption coefficient (from the line shape fit to the observed spectrum) and $\widetilde{\nu}_0$ is the transition wave number. Measured values of n and $\mathcal{A}$ enable calculation of the line intensity via the relation $S(T) = \mathcal{A}/n$. All line intensities reported here are corrected to the reference temperature $T_r = 296$ K using

$$S(T_r) = S(T)\frac{q(T)}{q(T_r)} \times \frac{e^{-hcE''/(k_b T_r)}}{e^{-hcE''/(k_b T)}}, \qquad (1)$$

where h is the Planck constant, $q(T)$ is the total internal partition function, and E'' is the lower state energy level (wave number units). Both $q(T)$ and E'' were taken from the 2004 edition of the HITRAN database [31].

III. EXPERIMENTAL RESULTS AND DISCUSSION

We chose to investigate 15 water vapor transitions within the wave number region between 7170 and 7183 cm^{-1}, having line intensities in the range from about 1.5×10^{-20} to 2.7×10^{-23} cm^{-1}/(molecule cm^{-2}). The complete list of transitions investigated in this paper together with their wave numbers, intensities, lower state energies, and quantum numbers reported in the HITRAN database is given in Table I. In this study all reported transitions are for the $H_2^{16}O$ isotopologue, and the reported intensities are effectively weighted for natural isotopic abundance of this water isotopologue which is equal to 0.997 317 [32].

To minimize systematic error in the water vapor sample preparation, we measured the background water vapor molar fraction associated with outgassing from the connecting tubing and/or ring-down cell. We purged the ring-down cell for several days with a molecular-sieve purified nitrogen "zero-
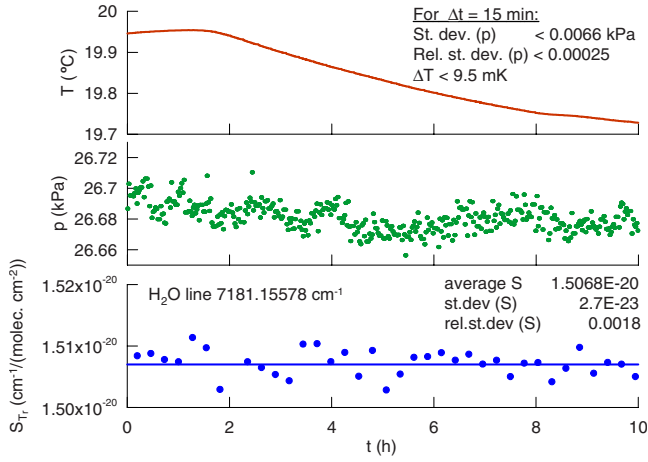
FIG. 2. (Color online) Ring-down cell temperature T, pressure p, and measured line intensities $S(T_r)$ as a function of time.

gas" stream ($x_w < 0.5$ nmol mol^{-1}), and we measured the residual water vapor in the ring-down cell by FS-CRDS of the $\tilde{\nu}_0 = 7181.155\,78$ cm^{-1} transition. We found that the background water vapor molar fraction was approximately 4 nmol mol^{-1}. This background level corresponds to a 0.12% relative uncertainty in line intensity for the 7181.155 78 cm^{-1} transition and a relative uncertainty $<0.03\%$ for all other transitions considered here.

In Fig. 2 the measured temperature and pressure in the ring-down cell over a 10 h time period are presented. During this time spectra of the 7181.155 78 cm^{-1} line broadened by 26.7 kPa (200 Torr) of nitrogen were measured. The time required to record one spectrum was about 15 min. In the bottom graph of Fig. 2 the intensity S of the measured line is presented as a function of time. These values are corrected to the reference temperature T_r as discussed above. The results presented in Fig. 2 demonstrate our measurement precision. For 15 min time periods, corresponding to the acquisition of a single spectrum, the cell temperature change is smaller than 9.5 mK. The pressure measurements indicate statistical (random) noise rather than systematic changes and the standard deviation of p over one spectrum acquisition is <6.7 Pa (0.05 Torr), which corresponds to a relative standard deviation of p smaller than 2.5×10^{-4}. As can be seen in the plot of line intensities vs time the measured intensities are not correlated with slow cell temperature or pressure drift. For this case the relative standard deviation of the measured line intensity is 1.8×10^{-3}.

In order to find a line shape model that properly fits our experimental spectra four different models were fitted: the commonly used Voigt profile (VP), the Galatry profile (GP) [33] which takes collisional (Dicke) narrowing into account using the soft-collision approximation, the speed-dependent Voigt profile (SDVP) [34] which accounts for the fact that collisional broadening and shifting effects depend on the absorber-perturber speed, and the speed-dependent Nelkin-Ghatak profile (SDNGP) [35,36] (also called the speed-dependent Rautian profile). This profile takes into account collisional narrowing and the speed dependence of collisional broadening and shifting. The collisional narrowing effect in the SDNGP model is treated in the hard-collision approximation. Here we chose the profile based on the hard-collision approximation because its form is simpler than the corresponding soft-collision version (speed-dependent Galatry profile) or the relatively complicated billiard-ball collision model (speed-dependent billiard-ball profile) (see [37] and references therein). All of these profiles were used before by many authors and in some cases for near-infrared water spectra. For both the SDVP and SDNGP the speed dependence of collisional broadening and shifting was modeled by a quadratic function as described by Priem *et al.* [38]. In this model we have two parameters a_W and a_S, which describe the speed dependence of the collisional broadening and shifting, respectively. They were found from the best fit of profiles to experimental data.

A description of semiclassical line shape models used in this paper can be found in Ref. [39]. We give only an expression for the SDNGP with quadratic speed-dependence functions to facilitate use of the experimental line shape parameters reported herein. The intensity distribution of an isolated spectral line can be written as the real part of the complex line shape function,

$$I(\nu) = \text{Re}\, \mathcal{I}(\nu). \tag{2}$$

For the SDVP the complex line shape function can be expressed in terms of an integral over the absorber's velocity distribution as

$$\mathcal{I}_{\text{SDVP}}(u) = \frac{2}{\pi^{3/2}} \int_{-\infty}^{\infty} dx e^{-x^2} x \left\{ \arctan\left(\frac{u - dB_S(x) + x}{gB_W(x)} \right) + \frac{i}{2} \ln\left[1 + \left(\frac{u - dB_S(x) + x}{gB_W(x)} \right)^2 \right] \right\}, \tag{3}$$

where x is the reduced absorber velocity, $u = (\nu - \nu_0)/\nu_D$, $g = \Gamma/\nu_D$, and $d = \Delta/\nu_D$. Here ν_0 is the unperturbed line center frequency, Γ and Δ are the collisional width [half width at half maximum (HWHM)] and shift, respectively, and $\nu_D = \gamma_D/(2\sqrt{\ln 2})$, where γ_D is the Doppler width [full width at half maximum (FWHM)] of the line. $B_W(x)$ and $B_S(x)$ are the reduced speed-dependent collisional width and shift functions [40] which in the case of quadratic speed dependence can be written as

$$B_W(x) = 1 + a_W(x^2 - 3/2), \tag{4}$$

$$B_S(x) = 1 + a_S(x^2 - 3/2). \tag{5}$$

For the SDNGP the complex line shape function has the following form:

$$\mathcal{I}_{\text{SDNGP}}(u) = \frac{\mathcal{I}_{\text{SDVP*}}(u)}{1 - \pi z \mathcal{I}_{\text{SDVP*}}(u)}, \tag{6}$$

where $z = \nu_{opt}/\nu_D$ and $\mathcal{I}_{\text{SDVP*}}(u)$ is $\mathcal{I}_{\text{SDVP}}(u)$ with $gB_W(x)$ replaced by $gB_W(x) + z$. The frequency of optical collisions ν_{opt} quantifies the collisional narrowing effect.

Figure 3 presents the experimental profile of the 7179.752 01 cm^{-1} line broadened by 13.3 kPa (100 Torr) of nitrogen. Below are the residuals $R(\nu)$ corresponding to respective fits of model line shapes: VP, GP, SDVP, and SD-NGP. For all profiles the Doppler width of the line was con-
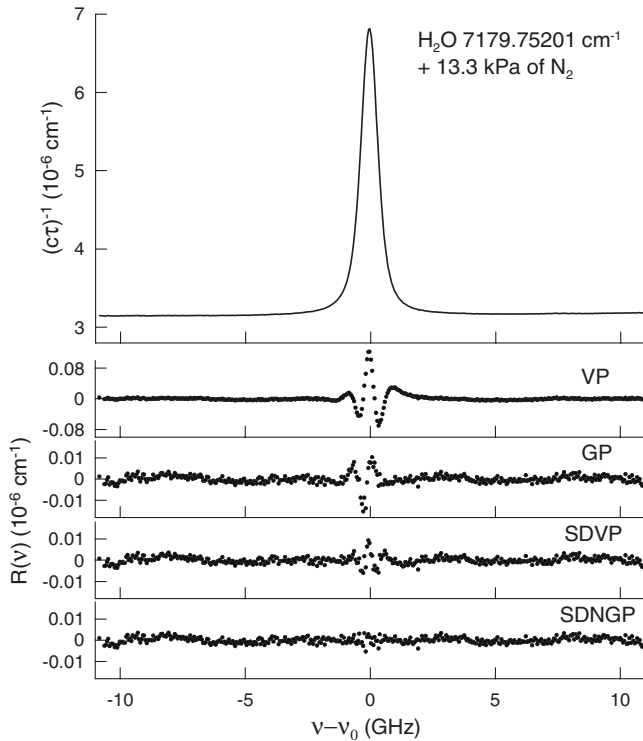
FIG. 3. Experimental profile of the H_2O 7179.752 01 cm^{-1} line broadened by 13.3 kPa of nitrogen and residuals corresponding to fits of model line shapes: VP, GP, SDVP, and SDNGP.

strained to the value calculated from the measured cell temperature. The collisional width and collisional narrowing parameters for the GP and SDNGP were fitted. The collisional shifting was constrained to the value for shifting by air (given in HITRAN) because N_2-induced shifting coefficients are not available in the literature for the transitions investigated here. The unperturbed line position ν_0 and both of the quadratic speed-dependence parameters a_W and a_S were also fitted. The line narrowing effect is clearly seen in the VP residuals and the fit quality can be greatly improved when a single narrowing effect (Dicke narrowing—GP or speed dependence of pressure broadening—SDVP) is taken into account. However, only when both the speed-dependence and Dicke narrowing are modeled together (SDNGP) do the fits give residuals having only random noise.

Fitting individual profiles with the SDNGP or any other profile that has two variable parameters corresponding to collisional narrowing and speed dependence of collisional broadening leads to an additional difficulty caused by correlation of these two parameters. As a result, one obtains a nonlinear dependence of these parameters with pressure and increased uncertainty in their fitted values. For the problem of nonlinear increase in collisional narrowing with pressure which was reported earlier by many authors, e.g., [41–43], the best remedy would be to constrain the speed dependence of collisional broadening to the calculated values if available. Unfortunately for the water lines investigated in this paper such data are unavailable. Also, the collisional narrowing parameter cannot be easily calculated and constrained in the fitting procedure because (as been demonstrated in many cases including water spectra) the value of ν_{opt} cannot be
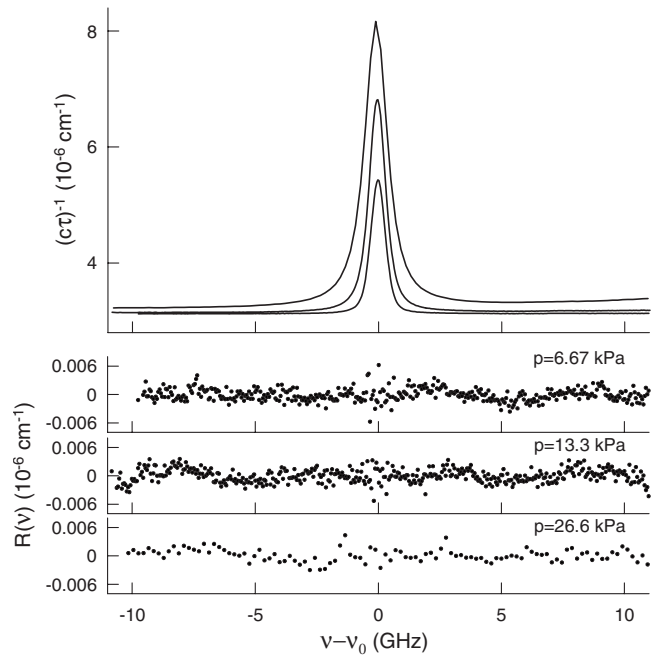
FIG. 4. Experimental profiles of the H_2O 7179.752 01 cm^{-1} line broadened by N_2 for nitrogen pressures 6.67, 13.3, and 26.6 kPa and water mole fraction $x_w = 1.8 \times 10^{-4}$ and residuals corresponding to the multispectrum fit of the SDNGP. In the top panel pressure increases from bottom to top.

determined from the diffusion coefficient of the absorber within the buffer gas. This fact can be understood in the framework of semiclassical line shape theory and is attributed to correlations between phase- and velocity-changing collisions [35,44–46].

In this paper multispectrum fits spanning a range of pressure were done for all experimental data. This method of data analysis was used before by Benner *et al.* [47] and Pine and co-workers [48,49]. Here we simultaneously fit sets of profiles corresponding to different pressures by fitting the collisional broadening $\gamma = \Gamma/p$ and narrowing coefficients, $\beta = \nu_{opt}/p$, instead of the respective widths, Γ and ν_{opt}, for each pressure. The $\delta = \Delta/p$ values were constrained and the line centers ν_0 were fitted individually for each pressure. This approach ensures a linear dependence of the broadening and narrowing widths on pressure, and it eliminates the correlation of ν_{opt} and a_W because the former is proportional to pressure whereas the latter is independent of pressure. The problem of correlation between the speed dependence of Γ and collisional narrowing was analyzed before in [38,50].

In Fig. 4 we present experimental profiles of the 7179.752 01 cm^{-1} water vapor line broadened by nitrogen for $p = 6.67$, 13.3, and 26.6 kPa and $x_w = 1.8 \times 10^{-4}$. Below are the residuals obtained from the multispectrum fit of the SDNGP. The residuals do not reveal any systematic discrepancies between model and experimental data for all measured pressures. The same fit procedure was applied to spectra of the other water transitions investigated here. Any weak neighboring lines were also taken into account and in most cases their positions and relative intensities were constrained to values from HITRAN. In several cases their positions or intensities were fitted to achieve better residuals. In order to
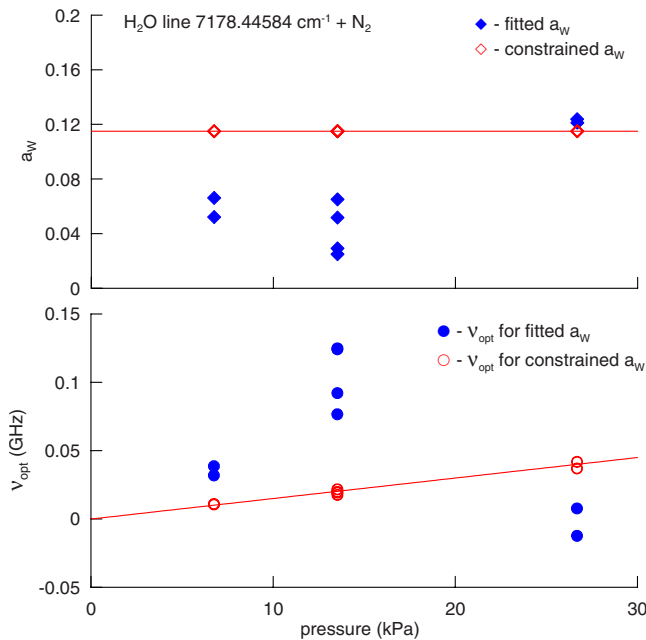
FIG. 5. (Color online) The speed-dependence parameter a_W and the collisional narrowing ν_{opt} vs pressure. The blue (solid) points correspond to parameters obtained from individual fits of SDNGP for each pressure with both a_W and ν_{opt} fitted. The red (open) points correspond to individual fits of SDNGP in which a_W was constrained to the value achieved from the multispectrum fit and ν_{opt} was fitted. Straight lines correspond to parameters from the multispectrum fits.

FIG. 6. (Color online) Fitted line area of the 7170.277 81 cm^{-1} water vapor line at 13.3 kPa of nitrogen as a function of length of spectrum for three different model profiles: VP, GP, and SDNGP.

properly model wings of strong lines we measured lines from the strongest to the weakest in the investigated region, enabling us to use our line intensities and line shape parameters. The relative line positions were taken from the HITRAN database.

An interesting test of the parameters resulting from the multispectrum fit is presented in Fig. 5. The upper and lower graphs show the variation in a_W and ν_{opt}, respectively, vs nitrogen pressure. The blue (solid) symbols correspond to parameters obtained from individual fits of the SDNGP for each pressure with both a_W and ν_{opt} fitted. The red (open) symbols correspond to individual fits of the SDNGP in which a_W was constrained to the value yielded by the multispectrum fit and ν_{opt} was fitted for each pressure. Straight lines correspond to parameters from the multispectrum fits. It is clearly seen that the fitted ν_{opt} depends linearly on pressure and the scatter in the fitted values is greatly reduced when a_W is constrained to be equal to the value determined from the multispectrum fit.

In Fig. 6 we present a comparison of the fitted line area of the $\tilde{\nu}_0 = 7170.277\,81$ cm^{-1} water vapor line at $p = 13.3$ kPa of nitrogen as a function of length of spectrum for three different model profiles: VP, GP, and SDNGP. Note that the FWHM of this transition is approximately 1.2 GHz at this pressure. As the spectrum length is reduced, systematic error in the line area grows, especially for the Voigt profile, because it fits the data poorly and there is less information about the line wings with reduced scan length. For a given spectrum length a better profile is needed to find the line area

properly. Even with a scan length that is more than 15 times the FWHM of the line, this plot clearly shows how inappropriate the Voigt profile is for quantitative water spectroscopy. The fitted line area is underestimated by 2–11% for this case, which is typical of many measurements. It is interesting that the Galatry profile is almost as good as the SDNGP for this line area determination. Also the line areas from the SDVP fits (not shown here) are very similar to those of the GP and SDNGP fits. This result agrees with the conclusions of Wehr *et al.* [51] who found that any profile giving a good quality of the fit also provides a good estimation of line area even if it is not physical. However, the clear advantage of the SD-NGP is that, contrary to the GP, one can find all the pressure-dependent width parameters to be linear with pressure. One should note that the difference in the VP line area and that of the GP or SDNGP may be smaller at higher pressures (for example, at atmospheric pressure) where the line shape is dominated by collisional broadening and the Doppler component is less important. Such a high pressure, however, is less convenient to use for quantitative spectroscopy because lines are blended and line mixing effects [52,53] often need to be taken into account. Moreover, the speed-dependent effects are also important for high pressures.

Table II summarizes our experimental results of water line intensities and line shape parameters based on the SDNGP fits. $\tilde{\nu}_{0_{HT}}$ is the transition wave number taken from HITRAN. S is our line intensity and $u(S)$ is the combined standard uncertainty of S, which takes into account the standard deviation of the fitted spectrum area and the measurement repeatability, as well as systematic (type B) uncertainties in the pressure and temperature measurements, LFPG and background water vapor molar fractions, and ring-down cavity free spectral range. Additionally in Table II, the systematic uncertainty associated with the line shape model was taken into account. From differences between the fitted line areas for the SDVP, GP, and SDNGP, we estimate an upper limit of 0.2% for the relative standard uncertainty arising from the choice of line shape. The component uncertainties for the respective transitions are plotted in Fig. 7 vs measured line intensity, where we have divided the combined uncertainty of line intensity into those due to water vapor sample preparation (LFPG output water vapor molar fraction, background

TABLE II. List of measured water vapor line intensities and line shape parameters from the SDNGP fits. $\tilde{\nu}_{0_{HT}}$—transition wave number in (cm^{-1}) from HITRAN 2004, S and $u(S)$—line intensity and its combined standard uncertainty in cm^{-1}/(molecule cm^{-2}), γ_{N_2} and $u(\gamma_{N_2})$—collisional broadening by N$_2$ (HWHM) and its combined standard uncertainty in (10^{-2} MHz/Pa), β_{N_2} and $u(\beta_{N_2})$—collisional narrowing coefficient and its combined standard uncertainty in (10^{-2} MHz/Pa), a_W and a_S—quadratic speed-dependence parameters of collisional broadening and shifting, $u(a_W)$ and $u(a_S)$ standard uncertainties of a_W and a_S, and $\delta_{air_{HT}}$—collisional shifting by air from HITRAN 2004 in (10^{-2} MHz/Pa). To convert γ and β coefficients to the more commonly used units of (cm^{-1} atm^{-1}), multiply the tabulated values by $10^{-2} \times 3.379\ 838\ 2$ (cm^{-1} atm^{-1})/(MHz Pa^{-1}).

$\tilde{\nu}_{0_{HT}}$	$S(T_r)$	$u(S)$	γ_{N_2}	$u(\gamma_{N_2})$	β_{N_2}	$u(\beta_{N_2})$	a_W	$u(a_W)$	a_S	$u(a_S)$	$\delta_{air_{HT}}$
7170.27781	2.0158×10^{-21}	7.4×10^{-24}	3.119	0.009	0.046	0.050	0.141	0.006	0.07	0.09	−0.2186
7172.69909	3.270×10^{-22}	2.3×10^{-24}	2.978	0.008	0.085	0.018	0.126	0.006	0.06	0.05	−0.1118
7173.96018	2.584×10^{-23}	1.6×10^{-25}	1.988	0.033	0.098	0.022	0.12	0.02	0.013	0.08	−0.3550
7174.13738	5.771×10^{-22}	1.7×10^{-24}	3.501	0.015	0.032	0.041	0.15	0.01	0.18	0.04	−0.3065
7175.49242	2.8062×10^{-23}	9.0×10^{-26}	2.798	0.009	0.134	0.027	0.10	0.02	0.14	0.02	−0.4429
7175.98676	2.6755×10^{-22}	7.8×10^{-25}	3.271	0.008	0.174	0.053	0.129	0.008	0.22	0.03	−0.2920
7178.44584	1.4419×10^{-22}	4.5×10^{-25}	3.031	0.010	0.150	0.012	0.115	0.001	0.11	0.08	−0.2246
7179.18718	5.761×10^{-23}	2.9×10^{-25}	3.226	0.035	0.280	0.035	0.12	0.015	0.006	0.005	−0.2414
7179.75201	2.3048×10^{-22}	7.1×10^{-25}	1.567	0.006	0.192	0.010	0.12	0.015	0.07	0.01	−0.4130
7180.39972	5.561×10^{-22}	2.0×10^{-24}	3.260	0.010	0.100	0.027	0.135	0.014	0.01	0.04	−0.1583
7180.61301	2.9491×10^{-23}	9.0×10^{-26}	2.140	0.010	0.173	0.033	0.12	0.02	0.02	0.06	−0.5326
7181.15578	1.5048×10^{-20}	6.1×10^{-23}	3.352	0.010	0.039	0.123	0.133	0.013	0.0	0.02	−0.3701
7182.20911	1.5785×10^{-21}	4.7×10^{-24}	3.611	0.007	0.162	0.031	0.14	0.008	0.02	0.03	−0.3423
7182.94962	3.772×10^{-21}	1.5×10^{-23}	3.251	0.016	0.170	0.118	0.124	0.016	0.10	0.09	−0.2565
7183.01579	4.069×10^{-22}	4.5×10^{-24}	3.18	0.12	0.170		0.124		0.10		−0.2565

water vapor molar fraction, temperature and pressure measurements) and those associated with the spectroscopic measurement of line area (line shape model, profile fitting, ring-down measurement reproducibility). It can be seen that the dominant uncertainty arises from the cavity ring-down measurement of line area where approximately half of this value comes from the estimated upper bound error caused by incomplete knowledge of the true line shape. Conversely, the water vapor sample preparation component contributes on the average only about one third of the combined uncertainty, and in the absence of spectroscopic measurement errors, we
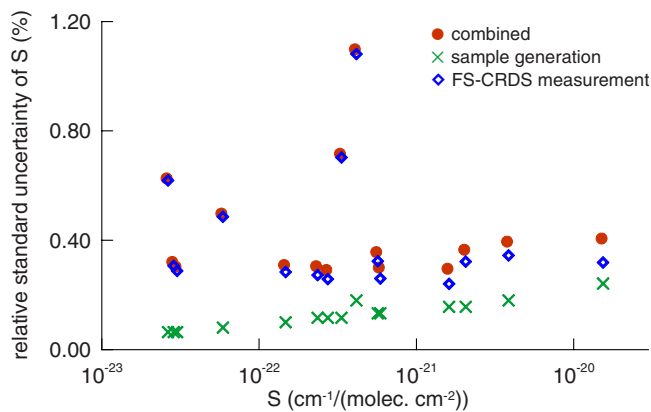
FIG. 7. (Color online) Relative combined standard uncertainty of the line intensities, and the respective contributions of the LFPG (sample generation) and spectroscopic measurement of peak area (FS-CRDS measurement). The latter two components are added in quadrature to give the combined uncertainty.

estimate that by using primary standards of humidity generation such as those implemented in this study, there would be a lower bound of ~0.15% for the relative uncertainty in line intensity. It is interesting to note that the relative combined standard uncertainty is less than 0.4% for the majority of the transitions reported here, which is arguably an unprecedented level of accuracy for water vapor rotation-vibration intensity measurements. Table II also gives the quantities γ_{N_2} and $u(\gamma_{N_2})$ which are the collisional broadening coefficient (HWHM) and its combined standard uncertainty, respectively, at the reference temperature T_r. Here the temperature exponent coefficients from HITRAN [31] were used for temperature correction of Γ. For all measured lines the temperature correction was between 0.5% and 0.8% of Γ. β_{N_2} and $u(\beta_{N_2})$ are the collisional narrowing coefficient ($\beta = \nu_{opt}/p$) and its combined standard uncertainty, respectively. a_W and a_S are the quadratic speed-dependence parameters of collisional broadening and shifting and $u(a_W)$ and $u(a_S)$ are their respective standard uncertainties. In the last column of Table II the coefficients of collisional shifting by air, taken from HITRAN and denoted by $\delta_{air_{HT}}$, are shown for completeness so that our fitted spectra can be reconstructed from the data. One should note that the experimental a_S parameters responsible for line asymmetry should be interpreted together with the pressure shifting δ coefficients that were assumed when fitting the spectra. As the assumed value of δ increases, the line asymmetry increases for a given value of a_S. In the last row of Table II there are no uncertainties for β_{N_2}, a_W, and a_S because these values were constrained to be the same as for neighboring lines, which were about ten times stronger in intensity and fitted together.

TABLE III. List of measured water vapor line shape parameters from GP fits. $\tilde{\nu}_{0_{HT}}$—transition wave number in (cm^{-1}) from HITRAN, γ_{N_2} and $u(\gamma_{N_2})$—collisional broadening by N_2 (HWHM) and its combined standard uncertainty in $(10^{-2}$ MHz/Pa), β_{N_2} and $u(\beta_{N_2})$—collisional narrowing coefficient, measured at $p = 13.3$ kPa, and its combined standard uncertainty in $(10^{-2}$ MHz/Pa). To convert γ and β coefficients to the more commonly used units of $(cm^{-1}$ atm$^{-1})$, multiply the tabulated values by $10^{-2} \times 3.379\,838\,2$ $(cm^{-1}$ atm$^{-1})/($MHz Pa$^{-1})$.

$\tilde{\nu}_{0_{HT}}$	$\gamma_{N_2}^{[GP]}$	$u(\gamma_{N_2}^{[GP]})$	$\beta_{N_2}^{[GP]}$	$u(\beta_{N_2}^{[GP]})$
7170.27781	3.085	0.009	1.581	0.032
7172.69909	2.953	0.011	1.436	0.029
7173.96018	1.966	0.012	0.923	0.009
7174.13738	3.427	0.033	1.853	0.046
7175.49242	2.788	0.018	1.003	0.008
7175.98676	3.235	0.010	1.701	0.024
7178.44584	3.011	0.015	1.409	0.023
7179.18718	3.18	0.03	1.607	0.049
7179.75201	1.551	0.007	0.871	0.013
7180.39972	3.233	0.010	1.726	0.069
7180.61301	2.11	0.05	1.090	0.010
7181.15578	3.316	0.009	1.797	0.028
7182.20911	3.569	0.009	2.147	0.049
7182.94962	3.225	0.013	1.686	0.076
7183.01579	3.31	0.03	1.686	

For comparison in Table III we present the collisional broadening $\gamma_{N_2}^{[GP]}$ and narrowing $\beta_{N_2}^{[GP]}$ coefficients, with their standard uncertainties $u(\gamma_{N_2}^{[GP]})$ and $u(\beta_{N_2}^{[GP]})$. These coefficients are for the same water lines as in Table II but obtained from fits of GPs to the experimental spectra. The values of $\beta_{N_2}^{[GP]}$ presented here were obtained from profiles measured at $p = 13.3$ kPa of nitrogen. The collisional broadening coefficients based on the GP fits are in most cases about 1% smaller than the respective coefficients based on SDNGP fits. It is worth noting that the collisional narrowing coefficients from the GP fits are 5–60 times bigger than the corresponding coefficients from the SDNGP fits. This result is not surprising because in fits of the Galatry profile the entire narrowing effect is interpreted to be a consequence of Dicke narrowing (which is described by the β coefficient), whereas in the SDNGP fits most of narrowing effect is attributed to the speed dependence of collisional width (described by the parameter a_W). We emphasize that because of the nonlinearity with pressure of the GP-fit-derived collisional narrowing, the $\beta_{N_2}^{[GP]}$ coefficients are valid only for a nitrogen pressure of 13.3 kPa and should not be extrapolated to different pressures. To quantify this effect we simulated spectral line shapes over the pressure range $p = 5-30$ kPa using the SDNGP line parameters in Table II for the $\tilde{\nu}_0 = 7181.155\,78$ cm^{-1} transition. We fit a series of Galatry profiles to the SDNGP profiles, subject to the constraint that $\nu_{opt} = p\beta_{N_2}^{[GP]}$. We found that the ratio of line areas (GP to SDNGP) decreased from 1.004 to 0.994, changing nearly linearly at a rate of $\sim -0.04\%$ kPa^{-1}. This simple calculation
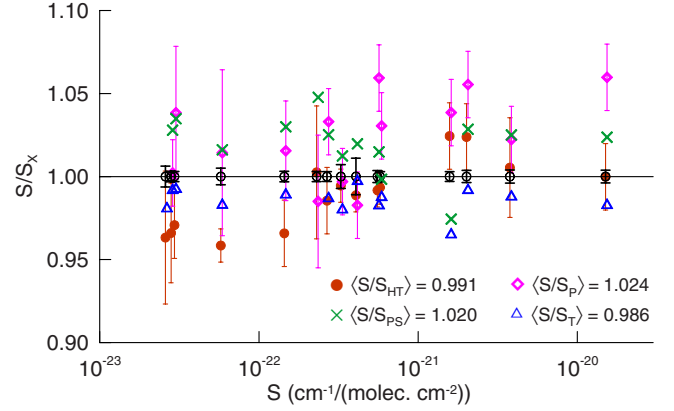
FIG. 8. (Color online) Ratios of our line intensities S to available experimental and theoretical values: HITRAN 2004 [31,54] S_{HT}, Parvitte et al. [55] S_P, Partridge and Schwenke [56] S_{PS}, and Tennyson [57] S_T as a function of line intensity S. Our results and their standard uncertainties are shown as black circles and error bars centered at unity on vertical axis.

illustrates that relatively large systematic errors in measured line area could be introduced by fitting a speed-dependent profile with a GP whose narrowing parameter is constrained to be linear with pressure.

In Fig. 8 we present ratios of our line intensities S to available experimental and theoretical values: HITRAN [31,54] S_{HT}, Parvitte et al. [55] S_P, Partridge and Schwenke [56] S_{PS}, and the recent calculations of Tennyson S_T [57]. Error bars correspond to the standard uncertainties $u(S)$ reported in [54,55]. Our results and their standard uncertainties are shown as black circles and error bars centered at unity on the vertical axis. The relative differences between our intensities and those of HITRAN, which were measured using Fourier transform spectroscopy, are between -4% and 2.5% and in most cases are within the combined standard uncertainties of these results. For weaker lines, (which correspond to higher J' quantum numbers) our line intensities are systematically smaller than the HITRAN values, the average ratio S/S_{HT} being 0.991. It is interesting to note that our measured line intensity for the strongest line in this spectral region ($\tilde{\nu}_{0_{HT}} = 7181.155\,78$ cm^{-1}) is in excellent agreement with the HITRAN value. The relative difference $(S - S_{HT})/S_{HT}$ is only $-1.5 \times 10^{-4} \pm 3.2 \times 10^{-3}$. Such a good agreement may be accidental, considering results for the other lines considered here. However confirmation of the commonly used HITRAN value is important for many applications because this transition is used in commercially available and widely used optical hygrometers [58,59]. Comparison with line intensities reported by Parvitte et al. [55] (denoted by S_P) that was obtained from diode laser spectroscopy reveals that our results are higher for most lines and the average ratio is $S/S_P = 1.024$. Theoretical values of line intensities given by Partridge and Schwenke [56], S_{PS}, are in most cases smaller than our values and the average ratio $S/S_{PS} = 1.02$. The most recent line intensities of Tennyson, S_T, calculated from CVR dipole moment surfaces [57] are systematically greater than our measured intensities by about 1.4%, and the standard deviation of the ratios of our measured intensities to those of
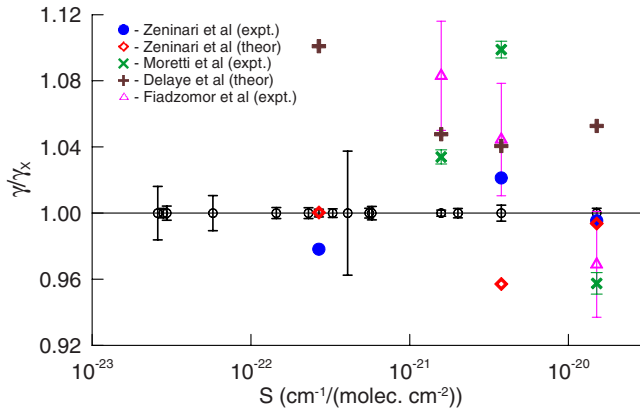
FIG. 9. (Color online) Ratios of our coefficients of collisional broadening by nitrogen γ_{N_2} to the corresponding data available in literature: Zéninari *et al.* [60] (experimental and theoretical results), Moretti *et al.* [61] (experimental), Delaye *et al.* [62] (theoretical), and Fiadzomor *et al.* [63] (experimental). Our results and their standard uncertainties are shown as black circles and error bars centered at 1 on vertical axis.

Tennyson is 0.8%, which is the smallest of all data sets considered here. This comparison does not include a lone outlier transition at $\tilde{\nu}_0 = 7179.752\,01$ cm^{-1} (see Fig. 3) in Tennyson's calculations which is ~22% lower than our measured value. Systematic differences between line intensities of stronger and weaker lines, which are observed for S/S_{HT} data, do not occur for the ratios given by S/S_P, S/S_{PS}, and S/S_T, which quantify our results relative to those of Parvitte *et al.* [55], Partridge and Schwenke [56], and Tennyson [57], respectively.

In Fig. 9 ratios of our coefficients of collisional broadening by nitrogen γ_{N_2} to the corresponding data available in literature are presented. Data reported by Zéninari *et al.* [60], both experimental and theoretical [marked as (expt.) and (theor.) in Fig. 9], are in best agreement with our results. Unfortunately there are only three lines available for comparison with our data. The sets of γ_{N_2} for only three lines reported by Moretti *et al.* [61] and by Fiadzomor *et al.* [63] seem to have a little bigger scatter. The theoretical pressure broadening coefficients of Delaye *et al.* [62] are systematically smaller than our γ_{N_2}. One should note that our γ_{N_2} were obtained from fits of the SDNGP to experimental profiles whereas the experimental data of Zéninari *et al.* [60], Moretti

et al. [61], and Fiadzomor *et al.* [63] were fitted with Voigt profiles. This difference in data analysis can lead to systematic differences in the fitted pressure broadening coefficients, which in some cases may be as big as a few percent (see e.g., [17,64]) and depend on experimental conditions.

IV. CONCLUSIONS

We have presented reference-grade line parameter measurements for rotation-vibration transitions of water vapor. These results were enabled by combining a primary humidity generation technique for sample preparation, a high-stability cavity ring-down spectroscopy method for accurate spectral measurements, and line shape models that incorporate collisional narrowing and speed-dependent broadening and line shifting effects. These data should serve as a reliable benchmark for validation of *ab initio* models of rotation-vibration spectra and for calibration of hygrometers employing laser absorption spectroscopy. For most cases the relative combined standard uncertainty in measured line intensity was <0.4%, half of which we assign to incomplete knowledge of the spectral line shape. Typically spectrum profile information (tabulated in line lists such as HITRAN) contains quantities sufficient to implement the Voigt profile. These include self- and air-broadening and shifting parameters and temperature exponents. Our results illustrate that the addition of three physically based parameters used with more advanced line shape models; the narrowing coefficient, the speed dependence of collisional broadening coefficient, and the speed dependence of collisional shifting coefficient substantially improve the prediction of line shape over a wide pressure range.

[1] M. T. Chahine, T. S. Pagano, H. H. Aumann, R. Atlas, C. Barnet, J. Blaisdell, Luke Chen, M. Divakarla, E. J. Fetzer, M. Goldberg, C. Gautier, S. Granger, S. Hannon, F. W. Irion, R. Kakar, E. Kalnay, B. H. Lambrigtsen, S.-Y. Lee, J. L. Marshall, W. W. McMillan, L. McMillin, E. T. Olsen, H. Revercomb, P. Rosenkranz, W. L. Smith, D. Staelin, L. Larrabee Strow, J. Susskind, D. Tobin, W. Wolf, and L. Zhou, Bull. Am. Meteorol. Soc. **87**, 911 (2006).

[2] H. Li, X. Zhou, J. B. Jeffries, and R. K. Hanson, Proc. Combust. Inst. **31**, 3215 (2007).

[3] V. Nagali and R. K. Hanson, Appl. Opt. **36**, 9518 (1997).

[4] X. Zhou, X. Liu, J. B. Jeffries, and R. K. Hanson, Meas. Sci. Technol. **14**, 1459 (2003).

[5] T. Cai, G. Wang, H. Jia, W. Chen, and G. Gao, Laser Phys. **18**, 1133 (2008).

[6] A. Farooq, J. B. Jeffries, and R. K. Hanson, Meas. Sci. Technol. **19**, 075604 (2008).

[7] H. H. Funke, B. L. Grissom, C. E. McGrew, and M. W. Raynor, Rev. Sci. Instrum. **74**, 3909 (2003).

[8] J. Yao, E. Olsen, M. Raynor, and G. D. Leonarduzzi, Solid State Technol. **50**, 46 (2007).

[9] P. V. Torek, D. L. Hall, T. A. Miller, and M. S. Wooldridge,

Appl. Opt. **41**, 2274 (2002).

[10] M. J. Thorpe, D. Balslev-Clausen, M. S. Kirchner, and J. Ye, Opt. Express **16**, 2387–2397 (2008).

[11] S. V. Shirin, N. F. Zobov, R. I. Ovsyannikov, O. L. Polyansky, and J. Tennyson, J. Chem. Phys. **128**, 224306 (2008).

[12] R. J. Barber, J. Tennyson, G. J. Harris, and R. N. Tolchenov, Mon. Not. R. Astron. Soc. **368**, 1087 (2006).

[13] L. Lodi, R. N. Tolchenov, J. Tennyson, S. V. Shirin, N. F. Zobov, O. L. Polyansky, G. Császár, J. N. P. van Stralen, and Lucas Visscher, J. Chem. Phys. **128**, 044304 (2008).

[14] D. Lisak, J. T. Hodges, and R. Ciurylo, Phys. Rev. A **73**, 012507 (2006).

[15] H. Tran, D. Bermejo, J. L. Domenech, P. Joubert, R. R. Gamache, and J.-M. Hartmann, J. Quant. Spectrosc. Radiat. Transf. **108**, 126 (2007).

[16] D. Lisak and J. T. Hodges, J. Mol. Spectrosc. **249**, 6 (2008).

[17] J. T. Hodges, D. Lisak, N. Lavrentieva, A. Bykov, L. Sinitsa, J. Tennyson, R. J. Barber, and R. N. Tolchenov, J. Mol. Spectrosc. **249**, 86 (2008).

[18] J. T. Hodges, H. P. Layer, W. W. Miller, and G. E. Scace, Rev. Sci. Instrum. **75**, 849 (2004).

[19] J. T. Hodges and R. Ciuryło, Rev. Sci. Instrum. **76**, 023112 (2005).

[20] G. E. Scace, P. H. Huang, J. T. Hodges, D. A. Olson, and J. R. Whetstone, in *Proceedings of the 1997 Workshop and Symposium of the National Conference of Standards Laboratories*, NCSL International, Boulder, Colorado, 1997), p. 657.

[21] J. T. Hodges and G. E. Scace, Micro. **24**, 59 (2006).

[22] J. T. Hodges and D. Lisak, Appl. Phys. B: Lasers Opt. **85**, 375 (2006).

[23] C. W. Meyer, J. T. Hodges, R. W. Hyland, G. E. Scace, J. Valencia-Rodriguez, and J. R. Whetstone, *Proceedings of the 5th International Symposium on Humidity and Moisture* (IN-METRO, Rio de Janeiro, 2007).

[24] A. Wexler, J. Res. NBS Monogr. **81A**, 5 (1977).

[25] R. W. Hyland and A. Wexler, in *1983 Annual Meeting in Washington, D.C. of the American Society of Heating, Refrigerating and Air-Conditioning Engineers* [ASHRAE Trans. **89**, 520 (1983)].

[26] G. E. Scace and J. T. Hodges, *Proceedings of the International Symposium on Temperature and Thermal Measurements in Industry and Science*, TEMPMEKO, 2001 (VDE, Berlin, 2002), p. 597.

[27] K. K. Lehmann, in *Cavity-Ringdown Spectroscopy: An Ultratrace-Absorption Measurement Technique*, edited by K. W. Busch and M. W. Busch (ACS, Washington, D.C., 1999), p. 106.

[28] D. Romanini and K. K. Lehmann, J. Chem. Phys. **99**, 6287 (1993).

[29] J. Zhang, Z. H. Lu, and L. J. Wang, Appl. Opt. **47**, 3143 (2008).

[30] D. J. Robichaud, J. T. Hodges, P. Masłowski, L. Y. Yeung, M. Okumura, C. E. Miller, and L. R. Brown, J. Mol. Spectrosc. **251**, 27 (2008).

[31] L. S. Rothman, D. Jacquemart, A. Barbe, D. C. Benner, M. Birk, L. R. Brown, M. R. Carleer, K. Chance, L. H. Coudert, V. Dana, V. M. Devi, J.-M. Flaud, R. R. Gamache, A. Goldman, J.-M. Hartmann, K. W. Jucks, A. G. Maki, J.-Y. Mandin, S. T. Massie, J. Orphal, A. Perrin, C. P. Rinsland, M. A. H. Smith, J. Tennyson, R. N. Tolchenov, R. A. Toth, J. V. Auwera,

P. Varanasi, and G. Wagner, J. Quant. Spectrosc. Radiat. Transf. **96**, 139 (2004).

[32] P. DeBièvre, M. Gallet, N. E. Holden, and I. L. Barnes, J. Phys. Chem. Ref. Data **13**, 809 (1984).

[33] L. Galatry, Phys. Rev. **122**, 1218 (1961).

[34] P. R. Berman, J. Quant. Spectrosc. Radiat. Transf. **12**, 1331 (1972).

[35] S. G. Rautian and I. I. Sobelman, Usp. Fiz. Nauk **90**, 209 (1966) [Sov. Phys. Usp. **9**, 701 (1967)].

[36] B. Lance, G. Blanquet, J. Walrand, and J.-P. Bouanich, J. Mol. Spectrosc. **185**, 262 (1997).

[37] R. Ciuryło, D. A. Shapiro, J. R. Drummond, and A. D. May, Phys. Rev. A **65**, 012502 (2001).

[38] D. Priem, F. Rohart, J. M. Colmont, G. Wlodarczyk, and J. P. Bouanich, J. Mol. Struct. **517**, 435 (2000).

[39] R. Ciuryło, Phys. Rev. A **58**, 1029 (1998).

[40] J. Ward, J. Cooper, and E. W. Smith, J. Quant. Spectrosc. Radiat. Transf. **14**, 555 (1974).

[41] P. Duggan, P. M. Sinclair, A. D. May, and J. R. Drummond, Phys. Rev. A **51**, 218 (1995).

[42] J. F. D'Eu, B. Lemoine, and F. Rohart, J. Mol. Spectrosc. **212**, 96 (2002).

[43] D. Lisak, G. Rusciano, and A. Sasso, Phys. Rev. A **72**, 012503 (2005).

[44] A. S. Pine, J. Chem. Phys. **101**, 3444 (1994).

[45] A. S. Pine, J. Quant. Spectrosc. Radiat. Transf. **62**, 397 (1999).

[46] R. Wehr, A. Vitcu, R. Ciurylo, F. Thibault, J. R. Drummond, and A. D. May, Phys. Rev. A **66**, 062502 (2002).

[47] D. C. Benner, C. P. Rinsland, V. Malathy Devi, M. A. H. Smith, and D. Atkins, J. Quant. Spectrosc. Radiat. Transf. **53**, 705 (1995).

[48] A. S. Pine and T. Gabard, J. Quant. Spectrosc. Radiat. Transf. **66**, 69 (2000).

[49] A. S. Pine and R. Ciuryło, J. Mol. Spectrosc. **208**, 180 (2001).

[50] F. Rohart, G. Wlodarczak, J.-M. Colmont, G. Cazzoli, L. Dore, and C. Puzzarini, J. Mol. Spectrosc. **251**, 282 (2008).

[51] R. Wehr, E. McKernan, A. Vitcu, R. Ciurylo, and J. R. Drummond, Appl. Opt. **42**, 6595 (2003).

[52] A. S. Pine, J. Quant. Spectrosc. Radiat. Transf. **57**, 145 (1997).

[53] G. D. Sheldon, P. M. Sinclair, M. P. Le Flohic, J. R. Drummond, and A. D. May, J. Mol. Spectrosc. **192**, 406 (1998).

[54] R. A. Toth, J. Quant. Spectrosc. Radiat. Transf. **94**, 51 (2005).

[55] B. Parvitte, V. Zéninari, I. Pouchet, and G. Durryet, J. Quant. Spectrosc. Radiat. Transf. **75**, 493 (2002).

[56] H. Partridge and D. W. Schwenke, J. Chem. Phys. **106**, 4618 (1997).

[57] J. Tennyson (private communication).

[58] Tiger Optics, 250 Titus Ave., Warrington, PA, (http://www.tigeroptics.com/).

[59] H. Abe and H. Kitano, Sens. Actuators, A **136**, 723 (2007).

[60] V. Zéninari, B. Parvitte, D. Courtois, N. N. Lavrentieva, Yu N. Ponomarev, and G. Durry, Mol. Phys. **102**, 1697 (2004).

[61] L. Moretti, A. Sasso, L. Gianfrani, and R. Ciuryło, J. Mol. Spectrosc. **205**, 20 (2001).

[62] C. Delaye, J. M. Hartmann, and J. Taine, Appl. Opt. **28**, 5080 (1989).

[63] P. A. Y. Fiadzomor, D. M. Baker, A. M. Keen, R. B. Grant, and A. J. Orr-Ewing, Appl. Spectrosc. **62**, 1354 (2008).

[64] D. Lisak and J. T. Hodges, Appl. Phys. B: Lasers Opt. **88**, 317 (2007).